

Polymorphism of CaTeO_3 and solid solutions
 $\text{Ca}_x\text{Sr}_{1-x}\text{TeO}_3$ Berthold Stöger,^a Matthias
Weil,^{a*} Erich Zobetz^a and Gerald
Giester^b^aInstitute for Chemical Technologies and Analy-
tics, Division of Structural Chemistry, Vienna
University of Technology, Getreidemarkt 9/164-
SC, A-1060 Vienna, Austria, and ^bInstitute for
Mineralogy and Crystallography, University of
Vienna, Althanstraße 14, A-1090 Vienna,
AustriaCorrespondence e-mail:
mweil@mail.zserv.tuwien.ac.atReceived 19 November 2008
Accepted 23 January 2009

Single crystals and microcrystalline samples of the calcium tellurate(IV) phases α -, β -, β' - and γ - CaTeO_3 as well as of two solid solutions $\text{Ca}_x\text{Sr}_{1-x}\text{TeO}_3$ ($x = 0.55$ and 0.77) have been synthesized and characterized by X-ray diffraction and thermal analysis. A comparative description of the structures and the relations between the polymorphs is given. The main building units of the hitherto unknown structures are isolated $[\text{Te}^{\text{IV}}\text{O}_3]^{2-}$ units and $[(\text{Ca},\text{Sr})\text{O}_x]$ ($x = 6-8$) polyhedra. All structures exhibit channels in which the Te^{IV} electron lone pairs protrude. The low-temperature phase α - CaTeO_3 is stable up to 1168 K. It exhibits nearly cylindrical channels (diameter ~ 4 Å) and differs structurally from the other phases, whereas the metastable high-temperature phases are closely related to each other. They feature oval channels (shortest and longest diameter ~ 2 and 8 Å). γ - CaTeO_3 can be described as an order–disorder (OD) structure of two non-polar layers with layer groups $p12_1/m1$ and $p12_11$. The γ - CaTeO_3 crystal under investigation consists of two polytypes with a maximum degree of order. The two phases $\text{Ca}_x\text{Sr}_{1-x}\text{TeO}_3$ ($x = 0.55$ and 0.77) are isostructural to the MDO_1 polytype of γ - CaTeO_3 . β - CaTeO_3 shows a distinct reversible phase transition at ~ 293 K. The low-temperature modification β' - CaTeO_3 as well as its high-temperature modification β - CaTeO_3 can be considered as threefold superstructures along $[100]$ based on the MDO_1 polytype of γ - CaTeO_3 .

1. Introduction

Materials that exhibit ferroelectric or nonlinear optical properties have extensive technical applications in the fields of capacitors, lasers, frequency doubling and other electric and optical devices. The basic prerequisite for such a class of compound is the existence of a polar direction without symmetrically equivalent directions [which occurs in the crystal classes 1, m , 2, $mm2$, 3, $3m$, 4, 6, $4mm$, $6mm$ (Hahn, 1983)], and the existence of a high polarizability and a strong preference for a particular stereochemistry. Possible building blocks for crystal engineering of these materials are oxoanions of the type $X\text{EO}_3^{n-}$ ($X = \text{As}^{\text{III}}$, S^{IV} , Te^{IV} , Se^{IV}), exhibiting a stereochemically active electron lone-pair E . For technological applications the desired materials must have both chemical and thermal stability over a wide temperature range, ruling out most of the arsenates(III), sulfates(IV) and selenates(IV) owing to easy hydrolysis, oxidation or thermal decomposition of these compounds. The most promising behaviour with respect to the desired stability ranges is for oxo-tellurate(IV) compounds, in particular the heavier homologues $M\text{TeO}_3$ of the alkaline earth elements, where $M = \text{Ca}, \text{Sr}, \text{Ba}$.

Indeed, CaTeO_3 (Rai *et al.*, 2002) and SrTeO_3 (Yamada & Iwasaki, 1972; Yamada, 1975) show ferroelectric properties and many research efforts have been devoted to measurements and the physico-chemical characterization of these materials, including reports on thermally induced phase transitions. The structures of four known SrTeO_3 polymorphs have been determined in the meantime (Elerman, 1993; Dityatiev *et al.*, 2006; Zavodnik *et al.*, 2007*a,b,c*, 2008), but it has not been possible until now to reliably determine the crystal structure of any of the reported CaTeO_3 polymorphs (Mishra *et al.*, 1998; Tripathi *et al.*, 2001).

In the present communication we discuss the crystal structures of four CaTeO_3 polymorphs and of two solid solutions with the chemical formula $\text{Ca}_x\text{Sr}_{1-x}\text{TeO}_3$, where $x = 0.55$ and 0.77 .

1.1. CaTeO_3 and closely related phases in the system Ca/Te/O

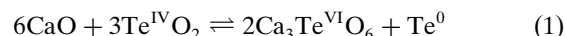
The first systematic investigations of phases with the composition CaTeO_3 date back to the mid-1960s. Independent studies reported the preparation and thermal behaviour of calcium tellurate(IV) starting from the hydrous phase $\text{CaTeO}_3 \cdot \text{H}_2\text{O}$ (Ivankova *et al.*, 1966), from the solid-state reaction of $\text{CaCO}_3/\text{TeO}_2$ mixtures (Malyutin *et al.*, 1969), or from the thermal decomposition of CaH_4TeO_6 , which also revealed a high-temperature modification above 1123 K (Knyaceva & Gushchina, 1968). In subsequent studies, Trömel & Ziethen-Reichenach (1970) reported two CaTeO_3 modifications stable at room temperature. However, none of the X-ray powder diffraction data reported in these publications were indexed. Some years later, dimorphism of CaTeO_3 at room temperature was also observed (Wroblewska *et al.*, 1979), but (unindexed) prominent reflections in the X-ray powder pattern deviated significantly from the previous investigation by Trömel & Ziethen-Reichenach (1970). The most recent experiments employing thermal analysis and X-ray powder diffraction methods (Mishra *et al.*, 1998; Tripathi *et al.*, 2001) revealed only one stable room-temperature modification (α - CaTeO_3) and two high-temperature polymorphs (β - and γ - CaTeO_3). The phase-transition temperatures from α - to β - and from β - to γ - CaTeO_3 were reported as 1155 and 1167 K (Tripathi *et al.*, 2001). The corresponding powder-diffraction patterns were indexed (Tripathi *et al.*, 2001) on the basis of triclinic (α), monoclinic (β) and hexagonal cells (γ). However, all derived cells are dubious because prominent reflections of the compound $\text{Ca}_4\text{Te}_5\text{O}_{14}$ with a very similar composition (ratio $\text{CaO}:\text{TeO}_2 = 4:5$ instead of 1:1) were used for indexing the three CaTeO_3 polymorphs. $\text{Ca}_4\text{Te}_5\text{O}_{14}$ was unknown during these investigations, but has been fully characterized in the meantime by single-crystal structure analysis (Weil, 2004). Therefore, it is most likely that a phase mixture consisting of various CaTeO_3 polymorphs and $\text{Ca}_4\text{Te}_5\text{O}_{14}$ instead of single CaTeO_3 phases were used for the indexing procedure (Tripathi *et al.*, 2001). A ferroelectric phase transition in CaTeO_3 at 293 K was reported by Rai *et al.* (2002).

Other phases in the Ca/Te/O system include the mixed-valent $\text{Te}^{\text{IV}}/\text{Te}^{\text{VI}}$ mineral carlfriesite, CaTe_3O_8 (Effenberger *et*

al., 1978), and the Te^{VI} compounds CaTeO_4 (Hottentot & Loopstra, 1979) and Ca_3TeO_6 (Hottentot & Loopstra, 1981; Burckhardt *et al.*, 1982). The structures of hydrous phases in the Ca/Te/O system have not yet been determined.

1.2. $(\text{CaO})_x \cdot (\text{TeO}_2)_y$ phases

Our experiments have shown that three thermodynamically stable crystalline phases with the composition $(\text{CaO})_x \cdot (\text{TeO}_2)_y$ exist at 973 K: CaTe_2O_5 , $\text{Ca}_4\text{Te}_5\text{O}_{14}$ and α - CaTeO_3 . Attempts to obtain phases with a $\text{CaO}:\text{TeO}_2$ ratio >1 always resulted in disproportionation of Te^{IV} according to



as was already noted by Trömel & Ziethen-Reichenach (1970). Even repeating the reaction with a large excess of Te in order to shift the equilibrium to the left side did not produce a measurable amount of any $(\text{CaO})_x \cdot (\text{TeO}_2)_y$ phase containing more than one equivalent of CaO. On the other hand, using more than two parts of TeO_2 per part CaO resulted in the formation of CaTe_2O_5 (Wroblewska *et al.*, 1979) and unreacted TeO_2 .

To our knowledge, of these three $(\text{CaO})_x \cdot (\text{TeO}_2)_y$ phases only the crystal structure $\text{Ca}_4\text{Te}_5\text{O}_{14}$ has yet been determined (Weil, 2004). The ditellurate(IV) CaTe_2O_5 was investigated by Redman *et al.* (1970), among others. Four different polymorphs were identified by powder diffraction, but structure elucidation has so far been unsuccessful since they crystallize in mica-like platelets with high stacking-fault probability, as do the Sr and Cd analogues. An unrelated non-twinned CaTe_2O_5 phase was recently obtained by hydrothermal synthesis (Weil & Stöger, 2008; Barrier *et al.*, 2008).

At temperatures above 1173 K compounds with a $\text{CaO}:\text{TeO}_2$ ratio <1 are unstable. Our thermogravimetry experiments showed that $\text{Ca}_4\text{Te}_5\text{O}_{14}$ slowly decomposes with the loss of TeO_2 in order to give CaTeO_3 . This fact can be used to obtain pure CaTeO_3 samples by using a small excess of TeO_2 . At elevated temperatures, the $\text{Ca}_4\text{Te}_5\text{O}_{14}$ formed will thereby slowly transform into CaTeO_3 .

2. Experimental

2.1. Preparation

TeO_2 , CaCO_3 and SrCO_3 were purchased from Merck (analytical grade) and used without further purification. CaO was prepared by heating CaCO_3 at 1123 K for 10 h. CaO/SrO mixtures were prepared by heating the corresponding $\text{CaCO}_3/\text{SrCO}_3$ mixtures at 1573 K for 12 h.

All experiments were performed in evacuated silica ampoules. At temperatures above 1000 K and when employing SrO, the samples were put into gold or alumina crucibles in order to prevent reaction with the wall of the ampoule. Quenching of reaction mixtures from different temperatures was performed in a cold-water bath. The reaction conditions of different runs are summarized in Table 1.

2.1.1. Microcrystalline material. Microcrystalline material was obtained by heating samples below the melting point. The

Table 1

Experimental details.

 The obtained powders were crystalline unless noted otherwise. Mass percentages according to Rietveld refinement (*FULLPROF*; Rodriguez-Carvajal, 1993).

Sample weight	Crucible	Temperature (K)	Time (h)	Remarks	Result
117.8 mg CaO, 319.2 mg TeO ₂	–	973	70	–	97% α -CaTeO ₃ , 3% Ca ₄ Te ₅ O ₁₄
123.4 mg CaO, 319.2 mg TeO ₂	–	973	70	–	95% α -CaTeO ₃ , 5% Ca ₃ TeO ₆
120.0 mg CaO, 319.2 mg TeO ₂	–	973	70	–	α -CaTeO ₃
120.0 mg CaO, 319.2 mg TeO ₂	Au	1273	70	Quenched	β -CaTeO ₃
60.0 mg CaO, 175.6 mg TeO ₂	Au	1273	70	Molten, quenched	91% γ -CaTeO ₃ (single crystals), 9% β -CaTeO ₃ (single crystals)
60.0 mg CaO, 175.6 mg TeO ₂	Au	1273	70	Molten, quenched, small crucible, 10 mg sample weight	γ -CaTeO ₃ (single crystals)
60.0 mg CaO, 175.6 mg TeO ₂	Al ₂ O ₃	1273	70	Molten, quenched	β -CaTeO ₃ (single crystals)
60.0 mg CaO, 175.6 mg TeO ₂	Al ₂ O ₃	1273–1000	70	Molten	α -CaTeO ₃ (single crystals), unknown phase
77.0 mg Ca _{0.67} Sr _{0.33} O, 159 mg TeO ₂	Au	1223	70	Molten, quenched	Ca _{0.77} Sr _{0.23} TeO ₃
85.5 mg Ca _{0.5} Sr _{0.5} O, 159 mg TeO ₂	Al ₂ O ₃	1223	70	Molten, quenched	Ca _{0.55} Sr _{0.45} TeO ₃
77.0 mg Ca _{0.67} Sr _{0.33} O, 190 mg TeO ₂	Al ₂ O ₃	1223–1170	70	Molten, quenched	Ca _{0.77} Sr _{0.23} TeO ₃ (single crystals), unknown phase
85.5 mg Ca _{0.5} Sr _{0.5} O, 190 mg TeO ₂	Al ₂ O ₃	1223–1170	70	Molten, quenched	Ca _{0.55} Sr _{0.45} TeO ₃ (single crystals), unknown phase

absence of impurities was monitored by X-ray powder diffraction of the ground bulk products.

Microcrystalline α -CaTeO₃ was obtained by heating a stoichiometric mixture of CaO and TeO₂ at 973 K for 70 h. Since the hygroscopic CaO had absorbed small amounts of water, multiple experiments were necessary to optimize the amount of CaO in order to obtain single-phase material.

Microcrystalline β -CaTeO₃ was obtained by quenching a mixture of CaO and TeO₂, which was heated in either a gold or an alumina crucible at 1273 K for 70 h.

Microcrystalline Ca_xSr_{1-x}TeO₃ phases were obtained by replacing CaO with the corresponding CaO:SrO mixture, heating at 1223 K for 70 h and quenching the reaction.

2.1.2. Single crystals. Single crystals were grown from melts, which resulted from using excess TeO₂, and were isolated by gentle crushing of chunks between two glass slides.

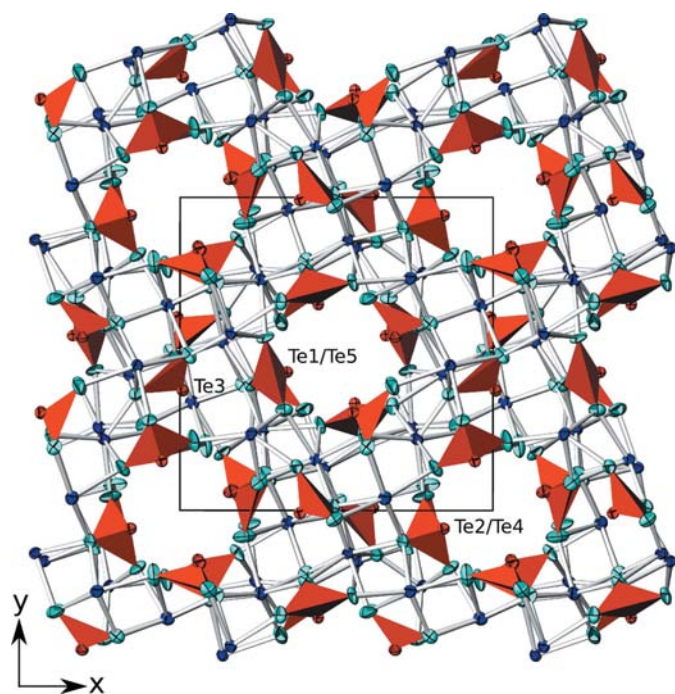
Single crystals of α -CaTeO₃ were obtained by heating a CaO:TeO₂ mixture with a 10% excess of TeO₂ at 1273 K and slowly cooling to 1000 K over the course of 70 h.

A mixture of single crystals of β -CaTeO₃ and γ -CaTeO₃ was obtained by heating the same mixture to 1273 K over the course of 70 h and by quenching the reaction. When small gold crucibles (6 mm diameter, 1 mm height) and little sample weight (less than 10 mg) were used, the sample contained only γ -CaTeO₃. With alumina crucibles (20 × 3 mm, 2 mm wall thickness) single-phase β -CaTeO₃ was obtained.

Single crystals of the composition Ca_xSr_{1-x}TeO₃ ($x = 0.55$ and $x = 0.77$) were obtained in the same way by replacing CaO with the corresponding CaO:SrO mixture with ratios of 1:1 and 2:1.

2.2. X-ray powder diffraction

Measurements of the ground bulk products were performed on a Philips X'Pert Pro diffractometer system [Cu K α _{1,2} radiation ($\lambda = 1.54060, 1.54439$ Å) equipped with an X'Celerator multi-channel detector, Bragg–Brentano geometry, silicon single-crystal sample holder, 5–70° 2 θ , 2.546° scan length (2 θ), 24.765 s per scan length]. The scans were converted into 0.02° step-size bins.


Figure 1

The crystal structure of α -CaTeO₃ viewed down [001]. [Te^{IV}O₃] units and Te atoms are given in red, Ca atoms are dark blue and O atoms light blue. Displacement ellipsoids represent 90% probability levels.

Table 2

Crystal data and details of the refinements of α - and γ -CaTeO₃ and the mixed Ca/Sr phases Ca_{0.77}Sr_{0.23}TeO₃ and Ca_{0.55}Sr_{0.45}TeO₃.

	α -CaTeO ₃	γ -CaTeO ₃	Ca _{0.77} Sr _{0.23} TeO ₃	Ca _{0.55} Sr _{0.45} TeO ₃
Crystal data				
Chemical formula	CaTeO ₃	CaTeO ₃	Ca _{0.77} Sr _{0.23} TeO ₃	Ca _{0.55} Sr _{0.45} TeO ₃
M_r	215.68	215.68	226.61	236.91
Cell setting, space group	Tetragonal, $P4_3$	Monoclinic, $P2_1$ ($P2_1/c$)	Monoclinic, $P2_1$	Monoclinic, $P2_1$
Temperature (K)	295	295	295	295
a, b, c (Å)	12.1070 (10), 12.1070 (10), 11.0911 (18)	8.4010 (17), 5.6913 (11), 11.340 (3) [22.680 (5)]	8.4941 (6), 5.7368 (4), 11.4562 (8)	8.5689 (17), 5.7805 (11), 11.553 (2)
β (°)	90	110.82 (3)	110.0810 (10)	109.975 (3)
V (Å ³)	1625.7 (3)	506.8 (2) [1013.6 (3)]	524.31 (6)	537.83 (18)
Z	20	6 (12)	6	6
D_x (Mg m ⁻³)	4.406	4.240	4.306	4.389
Radiation type	Mo $K\alpha$	Mo $K\alpha$	Mo $K\alpha$	Mo $K\alpha$
μ (mm ⁻¹)	10.52	10.12	12.92	15.47
Crystal form, colour	Fragment, colourless	Fragment, colourless	Fragment, colourless	Fragment, colourless
Crystal size (mm)	0.06 × 0.06 × 0.02	0.10 × 0.08 × 0.05	0.18 × 0.12 × 0.07	0.30 × 0.06 × 0.03
Data collection				
Diffractometer	SMART APEX	SMART APEX	SMART APEX	SMART APEX
Data collection method	ω scans	ω scans	ω scans	ω scans
Absorption correction	SADABS	SADABS	SADABS	SADABS
T_{\min}, T_{\max}	0.571, 0.817	0.431, 0.632	0.205, 0.465	0.090, 0.654
No. of measured, independent and observed reflections	18 973, 4932, 4591	11 577, 5987, 5480	5866, 2996, 2958	6223, 3266, 3222
Criterion for observed reflections	$I > 2\sigma(I)$	$I > 2\sigma(I)$	$I > 2\sigma(I)$	$I > 2\sigma(I)$
R_{int}	0.042	0.032	0.023	0.021
θ_{max} (°)	30.5	30.5	31.0	31.0
Refinement				
Refinement on	F^2	F^2	F^2	F^2
$R[F^2 > 2\sigma(F^2)], wR(F^2), S$	0.030, 0.058, 1.02	0.044, 0.099, 1.20	0.019, 0.045, 1.08	0.019, 0.045, 1.06
No. of reflections	4932	5987	2996	3266
No. of parameters	226	187	141	141
Weighting scheme	$\omega = 1/[\sigma^2(F_o^2) + (0.0238P)^2]$, where $P = (F_o^2 + 2F_c^2)/3$	$\omega = 1/[\sigma^2(F_o^2) + (0.0228P)^2 + 6.4447P]$, where $P = (F_o^2 + 2F_c^2)/3$	$\omega = 1/[\sigma^2(F_o^2) + (0.0172P)^2 + 0.2737P]$, where $P = (F_o^2 + 2F_c^2)/3$	$\omega = 1/[\sigma^2(F_o^2) + (0.0175P)^2 + 0.3278P]$, where $P = (F_o^2 + 2F_c^2)/3$
$(\Delta/\sigma)_{\text{max}}$	0.001	0.080	0.002	0.001
$\Delta\rho_{\text{max}}, \Delta\rho_{\text{min}}$ (e Å ⁻³)	1.60, -0.91	2.00, -1.74	0.65, -0.86	0.74, -0.86
Absolute structure	Flack (1983)	–	–	–
Flack parameter	0.05 (3)	–	–	–
Extinction method	–	SHELXL	SHELXL	SHELXL
Extinction coefficient	–	–	0.0091 (3)	0.0082 (3)
Twin (polytype) volume fractions	–	[19.8:80.2 (2)]	49:51 (2)	49.8:50.2 (9)

2.3. Single-crystal diffraction

Reflection intensities of single crystals of α -CaTeO₃, γ -CaTeO₃ and Ca_{*x*}Sr_{1-*x*}TeO₃ ($x = 0.55$ and 0.77) were collected at 295 K using the ω -scan technique with 0.3° rotation width on a SMART APEX three-circle diffractometer equipped with a CCD camera (Bruker AXS; Mo $K\alpha$ radiation, $\lambda = 0.71073$ Å). Three independent sets of 600 frames were measured, thus scanning the whole reciprocal sphere with high redundancy.

Data of β - and β' -CaTeO₃ crystals were collected at 200, 250, 275, 295, 325 and 350 K on a Nonius Kappa-CCD four-circle diffractometer using the ω -scan technique with 2° rotation width on 414 frames in nine runs (Mo $K\alpha$ radiation, $\lambda = 0.71073$ Å). Cooling and heating was performed by a stream of nitrogen using a Cryostream 600 (Oxford Cryosystems).

More details of the various data collections are summarized in Tables 2, 3 and 4.

2.4. Thermal analysis

α -CaTeO₃ was subjected to simultaneous TG (thermogravimetry)/DSC (differential scanning calorimetry) experiments on a NETZSCH 409 PC Luxx Thermobalance in a Pt crucible under Ar atmosphere. The sample was heated at a rate of 10 K min⁻¹ from room temperature to 1423 K and subsequently cooled down to room temperature at the same rate.

Low temperature (233–273 K) DSC measurements of α -, β -, β' - and γ -CaTeO₃ were performed on a NETZSCH DSC 204 FI Phoenix Differential Scanning Calorimeter.

2.5. Structure determinations and refinements

All structures were solved by direct methods and refined with the SHELXTL program package (Sheldrick, 2008). Absorption corrections were performed using a multi-scan approach with SADABS (Bruker, 2004), except for high- and

Table 3
Crystal data and details of the refinements of β -CaTeO₃.

	β -CaTeO ₃ (275 K)	β -CaTeO ₃ (295 K)	β -CaTeO ₃ (325 K)	β -CaTeO ₃ (350 K)
Crystal data				
Chemical formula	CaTeO ₃	CaTeO ₃	CaTeO ₃	CaTeO ₃
M_r	215.68	215.68	215.68	215.68
Cell setting, space group	Triclinic, $P1$	Triclinic, $P1$	Triclinic, $P\bar{1}$	Triclinic, $P\bar{1}$
Temperature (K)	275	295	325	350
a, b, c (Å)	25.6201 (4), 10.2408 (2), 11.3279 (2)	25.6220 (4), 10.2426 (2), 11.3327 (2)	25.6231 (4), 10.2467 (2), 11.3413 (2)	25.6225 (9), 10.2491 (4), 11.3482 (4)
α, β, γ (°)	107.2180 (10), 110.245 (2), 33.0160 (10)	107.2180 (10), 110.245 (2), 33.0190 (10)	107.2320 (10), 110.255 (2), 33.0200 (10)	107.2380 (10), 110.260 (2), 33.0220 (10)
V (Å ³)	1519.28 (5)	1520.42 (5)	1522.19 (5)	1523.47 (10)
Z	18	18	18	18
D_x (Mg m ⁻³)	4.243	4.240	4.235	4.232
Radiation type	Mo $K\alpha$	Mo $K\alpha$	Mo $K\alpha$	Mo $K\alpha$
μ (mm ⁻¹)	10.127	10.119	10.107	10.099
Crystal form, colour	Fragment, colourless	Fragment, colourless	Fragment, colourless	Fragment, colourless
Crystal size (mm)	0.12 × 0.08 × 0.03	0.12 × 0.08 × 0.03	0.12 × 0.08 × 0.03	0.12 × 0.08 × 0.03
Data collection				
Diffractometer	Nonius Kappa CCD	Nonius Kappa CCD	Nonius Kappa CCD	Nonius Kappa CCD
Data collection method	ω scans	ω scans	ω scans	ω scans
Absorption correction	Partial multi-scan	Partial multi-scan	Partial multi-scan	Partial multi-scan
T_{\min}, T_{\max}	0.376, 0.786	0.376, 0.786	0.377, 0.786	0.377, 0.786
No. of measured, independent and observed reflections	25 813, 25 813, 19 328	25 930, 25 930, 19 234	25 905, 13 856, 9848	25 949, 13 856, 9563
Criterion for observed reflections	$I > 2\sigma(I)$	$I > 2\sigma(I)$	$I > 2\sigma(I)$	$I > 2\sigma(I)$
R_{int}	–	–	0.052	0.052
θ_{max} (°)	36.28	36.28	36.20	36.28
Refinement				
Refinement on	F^2	F^2	F^2	F^2
$R[F^2 > 2\sigma(F^2)], wR(F^2), S$	0.053, 0.113, 1.04	0.051, 0.105, 1.04	0.051, 0.094, 1.12	0.043, 0.083, 1.02
No. of reflections	25 813	25 930	13 856	13 856
No. of parameters	543	813	417	417
Weighting scheme	$w = 1/[\sigma^2(F_o^2) + (0.0388P)^2 + 7.5688P]$, where $P = (F_o^2 + 2F_c^2)/3$	$w = 1/[\sigma^2(F_o^2) + (0.0372P)^2 + 2.6344P]$, where $P = (F_o^2 + 2F_c^2)/3$	$w = 1/[\sigma^2(F_o^2) + 11.7862P]$, where $P = (F_o^2 + 2F_c^2)/3$	$w = 1/[\sigma^2(F_o^2) + (0.0207P)^2 + 2.5034P]$, where $P = (F_o^2 + 2F_c^2)/3$
$(\Delta/\sigma)_{\text{max}}$	0.026	0.007	0.002	0.002
$\Delta\rho_{\text{max}}, \Delta\rho_{\text{min}}$ (e Å ⁻³)	3.58, -3.85	2.98, -3.53	2.36, -2.77	2.12, -1.91
Extinction method	<i>SHELXL</i>	<i>SHELXL</i>	<i>SHELXL</i>	<i>SHELXL</i>
Extinction coefficient	0.00091 (3)	0.00096 (3)	0.00116 (3)	0.00111 (3)
Twin volume fractions	46:54 (4)	45:55 (6)	–	–
s.o.f., O32a:O32b	–	–	39:61 (1)	38:62 (1)

low-temperature measurements of β - and β' -CaTeO₃, where the multi-scan approach based on the *HKL-SCALEPACK* program (Otwinowski *et al.*, 2003) was used. Unless noted otherwise, the displacement parameters of all atoms were refined anisotropically.

3. Crystal structures

3.1. Common features

All structures exhibit isolated distorted trigonal–pyramidal [Te^{IV}O₃]²⁻ units and [MO_{*x*}] ($M = \text{Ca, Sr}$) polyhedra ($x = 6\text{--}8$). β' -CaTeO₃ is an exception insofar as it contains a [TeO₃₊₁] unit, which is connected *via* a corner to a [TeO₃] unit. The trigonal–pyramidal shape of the [Te^{IV}O₃]²⁻ units is characteristic of three-coordinated Te^{IV} atoms (Zemann, 1971). All Te–O distances (Tables 5, 6 and 7) are in good agreement with the data given in a review on the crystal chemistry of oxotellurium(IV) compounds (Dolgikh, 1991). The lone-pair

electrons of the Te^{IV} atoms are stereochemically active and are located in channels and, in the case of α -CaTeO₃, also in enclosed cavities.

γ -CaTeO₃ will be discussed before β -CaTeO₃, because the structure of the latter can be described as a superstructure of the former.

3.2. α -CaTeO₃

α -CaTeO₃ features two crystallographically different nearly cylindrical channels (diameter ~ 4 Å) with rod group symmetry μ_4 running along 0, 0, z and $\frac{1}{2}, \frac{1}{2}, z$, respectively (Fig. 1). Each channel is delimited by two crystallographically different [Te^{IV}O₃]²⁻ units (Te1, Te5 and Te2, Te4) with the electron lone pair of the Te atoms oriented towards the centre of the channel (Fig. 2). A fifth [Te^{IV}O₃]²⁻ unit (Te3) is located between the channels with the electron lone-pair oriented into an enclosed cavity. These units are connected by two Ca atoms (Ca3 and Ca5) forming infinite chains along [001] with the rod

Table 4
Crystal data and details of the refinements of β' -CaTeO₃.

	β' -CaTeO ₃ (200 K)	β' -CaTeO ₃ (250 K)	β' -CaTeO ₃ (275 K)
Crystal data			
Chemical formula	CaTeO ₃	CaTeO ₃	CaTeO ₃
M_r	215.68	215.68	215.68
Cell setting, space group	Triclinic, $P\bar{1}$	Triclinic, $P\bar{1}$	Triclinic, $P\bar{1}$
Temperature (K)	200	250	275
a, b, c (Å)	25.5990 (5), 10.3871 (2), 11.2384 (3)	25.6149 (4), 10.3921 (2), 11.2440 (2)	25.6215 (5), 10.3933 (2), 11.2481 (2)
α, β, γ (°)	108.620 (1), 112.398 (2), 32.307 (2)	108.608 (1), 112.394 (2), 32.313 (1)	108.604 (9), 112.393 (13), 32.3190 (10)
V (Å ³)	1476.60 (6)	1479.25 (5)	1480.59 (5)
Z	18	18	18
D_x (Mg m ⁻³)	4.366	4.358	4.354
Radiation type	Mo $K\alpha$	Mo $K\alpha$	Mo $K\alpha$
μ (mm ⁻¹)	10.420	10.401	10.391
Crystal form, colour	Fragment, colourless	Fragment, colourless	Fragment, colourless
Crystal size (mm)	0.12 × 0.08 × 0.03	0.12 × 0.08 × 0.03	0.12 × 0.08 × 0.03
Data collection			
Diffractometer	Nonius Kappa CCD	Nonius Kappa CCD	Nonius Kappa CCD
Data collection method	ω scans	ω scans	ω scans
Absorption correction	Partial multi-scan	Partial multi-scan	Partial multi-scan
T_{\min}, T_{\max}	0.3678, 0.7451	0.3683, 0.7455	0.3686, 0.7812
No. of measured, independent and observed reflections	17 367, 12 498, 9708	25 122, 13 422, 10 123	25 213, 13 485, 10 052
Criterion for observed reflections	$I > 2\sigma(I)$	$I > 2\sigma(I)$	$I > 2\sigma(I)$
R_{int}	0.041	0.047	0.047
θ_{max} (°)	36.23	36.24	36.24
Refinement			
Refinement on	F^2	F^2	F^2
$R[F^2 > 2\sigma(F^2)], wR(F^2), S$	0.039, 0.086, 1.01	0.034, 0.066, 1.01	0.034, 0.068, 1.01
No. of reflections	12 498	13 422	13 485
No. of parameters	407	407	407
Weighting scheme	$w = 1/[\sigma^2(F_o^2) + (0.0352P)^2]$, where $P = (F_o^2 + 2F_c^2)/3$	$w = 1/[\sigma^2(F_o^2) + (0.0197P)^2]$, where $P = (F_o^2 + 2F_c^2)/3$	$w = 1/[\sigma^2(F_o^2) + (0.0210P)^2]$, where $P = (F_o^2 + 2F_c^2)/3$
$(\Delta/\sigma)_{\text{max}}$	0.003	0.005	0.004
$\Delta\rho_{\text{max}}, \Delta\rho_{\text{min}}$ (e Å ⁻³)	2.96, -2.40	2.06, -2.32	2.40, -2.12
Extinction method	SHELXL	SHELXL	SHELXL
Extinction coefficient	0.00066 (4)	0.00087 (3)	0.00085 (3)

symmetry group C_{2v} (Fig. 3). The different [Te^{IV}O₃]²⁻ units share corners and edges with five different irregular [CaO_x] ($x = 6-8$) polyhedra that fill the space between the channels, establishing a framework structure. The Ca—O distances range from 2.262 (4) to 3.033 (5) Å, which compares well with those observed for other structures in the Ca/Te^{IV}/O system, viz. CaTeO₄ (Hottentot & Loopstra, 1979), Ca₄Te₅O₁₄ (Weil, 2004) and CaTe₂O₅ (Barrier *et al.*, 2008; Weil & Stöger, 2008). Moreover, the average Ca—O distance of 2.46 Å is in good agreement with the value of 2.42 Å calculated from the sum of the ionic radii of O²⁻ and seven-coordinate Ca²⁺ given by Shannon (1976).

3.3. γ -CaTeO₃ and Ca_xSr_{1-x}TeO₃

3.3.1. Refinement. During refinement of γ -CaTeO₃ in $P2_1/c$ excessive residual electron density in the difference Fourier map was observed and could not be explained by a simple structure model. The three highest residual peaks were on positions $x' = x, y' = \frac{1}{2} - y, z' = z$ relative to a Te and two Ca atoms, suggesting a mirror plane normal to the y axis. Closer inspection revealed that γ -CaTeO₃ can be described as an OD structure and the residual electron density corresponds to a

minor polytype in the space group $P2_1$ with the basis vector c halved when compared with the major polytype.

In order to refine γ -CaTeO₃ with both polytype fractions, the lattice parameters of the polytype with the doubled cell volume ($P2_1/c$) and the space group $P2_1$, which is the largest common subgroup of $P2_1$ and $P2_1/c$, were used. In a first step, the $P2_1/c$ polytype was refined by pairs of atoms constrained to positions (x, y, z) and $(-x, -y, -z)$, thus obtaining the inversion symmetry missing in the overall structure. Moreover, the ADPs (anisotropic displacement parameters) of the corresponding atoms were constrained to be equivalent. Then, for parts of the structure where the two polytypes do not overlap (B layers in the description below), for the $P2_1$ polytype pairs of atoms constrained to positions (x, y, z) and $(x, y, \frac{1}{2} + z)$ and the same ADPs were added, thus taking into account the halved unit cell. Of the atoms in the minor polytype only the Ca atoms were refined anisotropically since some of the Te and O atoms gave physically meaningless values. The sum of the s.o.f. (site occupation factors) of atoms in both polytypes was constrained to 1. In the final difference-Fourier map no remarkable additional electron density was found.

On CCD frames collected from a γ -CaTeO₃ crystal, pseudo-precession photographs computed from those frame sets, and

Table 5
Selected atomic distances (Å) and angles (°) in α -CaTeO₃.

Te1—O9	1.839 (4)	Ca3—O2	2.296 (5)
Te1—O7	1.860 (5)	Ca3—O8	2.421 (5)
Te1—O8	1.871 (5)	Ca3—O1	2.430 (5)
Te2—O4	1.834 (4)	Ca3—O14	2.439 (4)
Te2—O5	1.844 (5)	Ca3—O15	2.449 (5)
Te2—O3	1.850 (4)	Ca3—O3	2.491 (5)
Te3—O6	1.880 (4)	Ca3—O4	2.643 (5)
Te3—O1	1.883 (4)	Ca4—O7	2.368 (5)
Te3—O2	1.890 (4)	Ca4—O1	2.415 (5)
Te4—O11	1.858 (4)	Ca4—O12	2.437 (5)
Te4—O10	1.879 (4)	Ca4—O3	2.448 (5)
Te4—O12	1.883 (4)	Ca4—O10	2.449 (5)
Te5—O13	1.861 (5)	Ca4—O2	2.516 (5)
Te5—O15	1.873 (4)	Ca4—O5	2.796 (5)
Te5—O14	1.874 (4)	Ca4—O8	3.033 (5)
Ca1—O6	2.262 (4)	Ca5—O9	2.391 (4)
Ca1—O8	2.370 (5)	Ca5—O6	2.399 (4)
Ca1—O4	2.380 (5)	Ca5—O7	2.428 (5)
Ca1—O15	2.394 (5)	Ca5—O13	2.429 (4)
Ca1—O11	2.395 (5)	Ca5—O1	2.440 (5)
Ca1—O12	2.407 (5)	Ca5—O10	2.441 (5)
Ca2—O3	2.317 (5)	Ca5—O2	2.461 (5)
Ca2—O5	2.325 (5)		
Ca2—O7	2.354 (5)		
Ca2—O13	2.390 (5)		
Ca2—O14	2.409 (4)		
Ca2—O10	2.432 (5)		
Ca2—O9	2.855 (6)		
O9—Te1—O7	93.7 (2)	O11—Te4—O10	96.2 (2)
O9—Te1—O8	103.2 (2)	O11—Te4—O12	103.5 (2)
O7—Te1—O8	98.1 (2)	O10—Te4—O12	101.0 (2)
O4—Te2—O5	100.2 (2)	O13—Te5—O15	97.50 (19)
O4—Te2—O3	93.7 (2)	O13—Te5—O14	100.3 (2)
O5—Te2—O3	92.9 (2)	O15—Te5—O14	101.45 (19)
O6—Te3—O1	97.1 (2)		
O6—Te3—O2	89.1 (2)		
O1—Te3—O2	92.39 (19)		

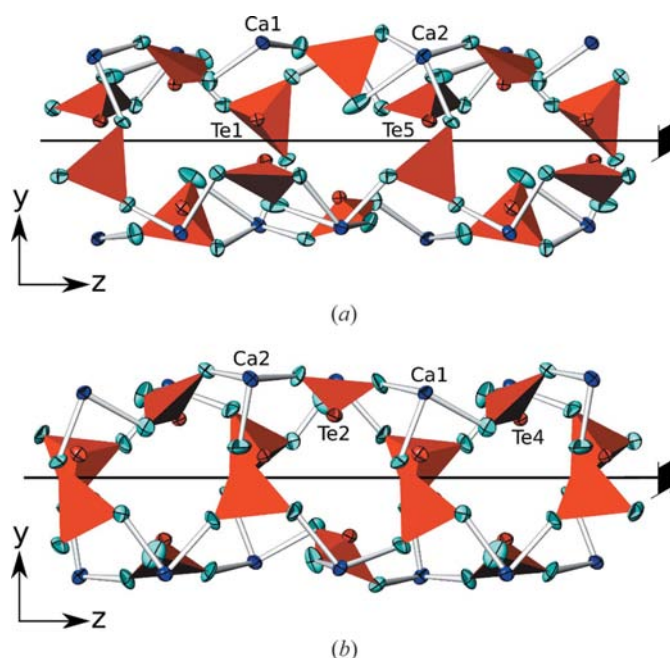


Figure 2
The two different channels in α -CaTeO₃, delimited by (a) Te1 and Te5, and (b) Te2 and Te4 (bottom), viewed down [100]. Colour codes and displacement ellipsoids as in Fig. 1. Graphical symmetry element symbols according to *International Tables for Crystallography*.

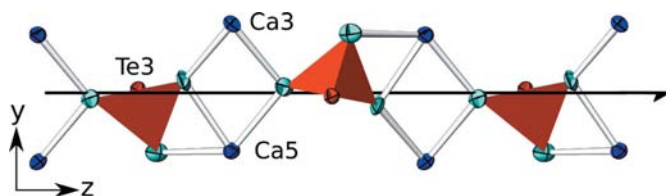


Figure 3
 α -CaTeO₃: ${}^1_{\infty}[\text{TeCa}_2\text{O}_3]^{2+}$ chain built of $[\text{Te}_3\text{O}_3]^{2-}$ units connected by Ca3 and Ca5 atoms with rod group symmetry μ_2 running along [001], as viewed down [100]. Colour codes, displacement ellipsoids and symbols as in Fig. 2.

likewise in line scans performed with a point detector, the reflections with $l = 2n$, corresponding to family reflections of the OD structure, are sharp, whereas those with $l = 2n + 1$ (characteristic reflections) show distinct broadening in [001], indicating disorder in the layer-stacking direction (Ferraris *et al.*, 2004).

Calculations have shown that polytypes with more complex stacking orders would produce pronounced reflections on the line segments [020, 022], [040, 042], [122, 126], [142, 146], [230, 234], [334, 338], [334, 338], [420, 424], [440, 444], [524, 52,10] and [544, 54,10] in reciprocal space (indexed with the $P2_1/c$ cell setting of the major polytype). However, no reflections with non-integer hkl values could be detected on these segments.

The closely related non-centrosymmetric structures of composition $\text{Ca}_x\text{Sr}_{1-x}\text{TeO}_3$ ($P2_1$) were refined as inversion twins with a twin ratio close to 1. The occupational disorder of the Ca and Sr atom was refined with the s.o.f. constrained to be equal to 1 for each metal site and common ADPs were used. The cell origin was chosen so that the y coordinates of the atoms are comparable to those in γ -CaTeO₃.

3.3.2. Structure. γ -CaTeO₃ and $\text{Ca}_x\text{Sr}_{1-x}\text{TeO}_3$ belong to a monoclinic/rectangular category IV OD family with two types of non-polar layers, *A* and *B*, parallel to (001) (Fig. 4, left). The OD groupoid family symbol reads according to the notation of Grell & Dornberger-Schiff (1982) as

$$\begin{array}{cc} A & B \\ p12_1/m1 & p12_1. \\ [0, 0] & \end{array} \quad (2)$$

The layer group notation is given according to Vol. E of the *International Tables for Crystallography* (Kopsky & Litvin, 2002). Layer names¹ deviating from the layer notation used by Grell & Dornberger-Schiff (1982) have been chosen for clarity. Te1 marks the boundary between both layers. Layers *A* (Te1, Te2, Ca2, O4–O6) and *B* (Te3, Ca1, Ca3, O1–O3, O7–O9) have layer symmetry $p12_1/m1$ and $p12_11$.

Given the position of a type *A* layer, adjacent layers of type *B* can appear in two enantiomorphic orientations with respect to [010], which we denote by B^+ and B^- . This is expressed by the NFZ relationship of OD theory, which is given as $Z = N/F$ (Đurovič, 1997), where $Z = 2$ is the number of

¹ According to Grell & Dornberger-Schiff (1982), layers *A* and *B* would be called A^1 and A^2 .

Table 6

Selected atomic distances (Å) and angles (°) in β - and β' -CaTeO₃, calculated from datasets measured at 350 and 200 K.

Ca–O distances and data for β - and β' -CaTeO₃ measured at other temperatures are given in the supplementary material.

	$\beta, x = 1$	$\beta, x = 2$	$\beta, x = 3$	$\beta', x = 1$	$\beta', x = 2$	$\beta', x = 3$
Te1x–O3x	1.857 (3)	–	1.859 (3)	1.855 (3)	1.884 (3)	1.861 (3)
Te1x–O3xB	–	1.805 (9)	–	–	–	–
Te1x–O1x	1.873 (3)	1.852 (4)	1.888 (3)	1.887 (3)	1.888 (3)	1.891 (3)
Te1x–O2x	1.877 (3)	1.827 (4)	1.882 (3)	1.875 (3)	1.865 (3)	1.887 (3)
Te1x–O3xA	–	1.915 (6)	–	–	–	–
Te2x–O4x	1.835 (3)	1.837 (3)	1.858 (3)	1.847 (3)	1.846 (4)	1.867 (3)
Te2x–O5x	1.852 (4)	1.839 (4)	1.843 (4)	1.842 (3)	1.859 (3)	1.909 (3)
Te2x–O6x	1.857 (3)	1.837 (3)	1.825 (4)	1.857 (3)	1.850 (4)	1.858 (3)
Te3x–O8x	1.853 (3)	1.859 (3)	1.848 (3)	1.882 (3)	1.859 (3)	1.864 (4)
Te3x–O9x	1.859 (3)	1.889 (3)	1.855 (3)	1.860 (3)	1.887 (3)	1.874 (3)
Te3x–O7x	1.862 (3)	1.896 (3)	1.851 (3)	1.883 (3)	1.898 (3)	1.846 (3)
O3x–Te1x–O1x	93.37 (14)	–	98.61 (14)	91.79 (15)	97.19 (14)	96.73 (14)
O3x–Te1x–O2x	101.34 (15)	–	101.21 (14)	101.10 (15)	99.74 (14)	100.83 (14)
O1x–Te1x–O2x	93.87 (14)	95.8 (2)	99.31 (14)	95.11 (14)	104.20 (14)	99.45 (14)
O32B–Te12–O22	–	112.9 (4)	–	–	–	–
O32B–Te12–O12	–	80.5 (4)	–	–	–	–
O22–Te12–O32A	–	84.1 (2)	–	–	–	–
O12–Te12–O32A	–	103.4 (2)	–	–	–	–
O4x–Te2x–O5x	103.04 (17)	104.96 (17)	94.51 (17)	103.59 (17)	99.82 (17)	91.63 (15)
O4x–Te2x–O6x	104.71 (16)	101.87 (16)	93.43 (17)	102.23 (16)	98.61 (19)	91.61 (15)
O5x–Te2x–O6x	92.45 (17)	94.86 (17)	103.4 (2)	92.03 (16)	99.17 (16)	102.89 (15)
O8x–Te3x–O9x	94.10 (15)	98.08 (14)	93.04 (16)	90.99 (15)	96.32 (15)	94.69 (16)
O8x–Te3x–O7x	92.66 (14)	92.71 (13)	95.97 (16)	93.45 (15)	92.17 (14)	98.76 (16)
O9x–Te3x–O7x	93.87 (14)	89.01 (14)	101.90 (15)	94.31 (14)	89.57 (14)	99.65 (15)

distinct positions of *B* layers given a fixed position of an *A* layer, $N = 2$ is the order of the group of λ - τ -POs of *A* layers ($G = p1m1$) and $F = 1$ the order of the group of those operations in *G*, which are also valid for adjacent layers *B* ($p1$). For layers of type *B*, on the other hand, $G = p1$, and hence $Z = N = F = 1$.

Consequently, two types of *BAB* layer triples (*viz.* B^+AB^+ and B^+AB^-) exist but only one type of *ABA* triples exist. These give rise to two possible stacking orders with maximum degree of order (Dornberger-Schiff & Grell, 1982), MDO₁ ($\dots AB^+AB^+ \dots$, $P2_1$, $\mathbf{c} = \mathbf{c}_0$) and MDO₂ ($\dots AB^+AB^- \dots$, $P2_1/c$, $\mathbf{c} = 2\mathbf{c}_0$). The schematized structures and local symmetry of the MDO₁ and MDO₂ polytypes are illustrated in Fig. 4 (right) by two types of triangles: red ones possessing a mirror plane normal to [010], blue ones exhibiting no mirror plane. The triangles are double-sided, the different sides being represented by bright and dark colours. For different γ -CaTeO₃ crystals an MDO₁:MDO₂ ratio of $\sim 2:8$ was determined in each case. In the Ca_xSr_{1-x}TeO₃ structures only MDO₂ exists.

The generating operation of MDO₁ is a translation along \mathbf{c}_0 . The 2₁ screw rotations of layers *A* and *B* are total operations of the whole structure. MDO₂ is generated by continuous application of a *c* glide. The glide plane coincides with the mirror plane of layers *A* at $y = \frac{1}{4}$. The 2₁ screw rotations of layers *B* and the inversion symmetry of layers *A* are total operations of the MDO₂ polytype.

In both MDO polytypes the mirror symmetry of the *A* layers is lost. Additionally, in MDO₁ their inversion centre is

lost, resulting in actual $p12_11$ symmetry for the *A* layers, whereas in MDO₂ the 2₁ screw axis is missing, resulting in $p\bar{1}$ symmetry. Layers of type *B*, on the other hand, retain their 2₁ screw axis in both MDO polytypes and have the same symmetry in the real MDO structures as well as in the OD interpretation.

Since the *A* layers in the OD approach have a higher symmetry than in the real structure, they have to be idealized. The idealized positions of atoms in the *A* layer were constructed by moving atoms that are located close to the mirror plane (with $y \simeq \frac{1}{4}$ or $y \simeq \frac{3}{4}$, *viz.* Ca2, Te1, Te2 and O4) onto the plane. For the two remaining atoms (O5 and O6), which are related by (pseudo-)mirror symmetry, an averaged atom has been constructed. Coordinates of the idealized structure are available in the supplementary materials.² The distances of the atomic positions calculated on the basis of single-crystal diffraction data from the atoms in the idealized structure are given in Table 8 for γ -CaTeO₃ and for Ca_xSr_{1-x}TeO₃.

The maximum deviation of only 0.108 Å for heavy atoms (Te or Ca/Sr) is a clear indication of the higher local symmetry of the *A* layer and therefore of the validity of the OD interpretation.

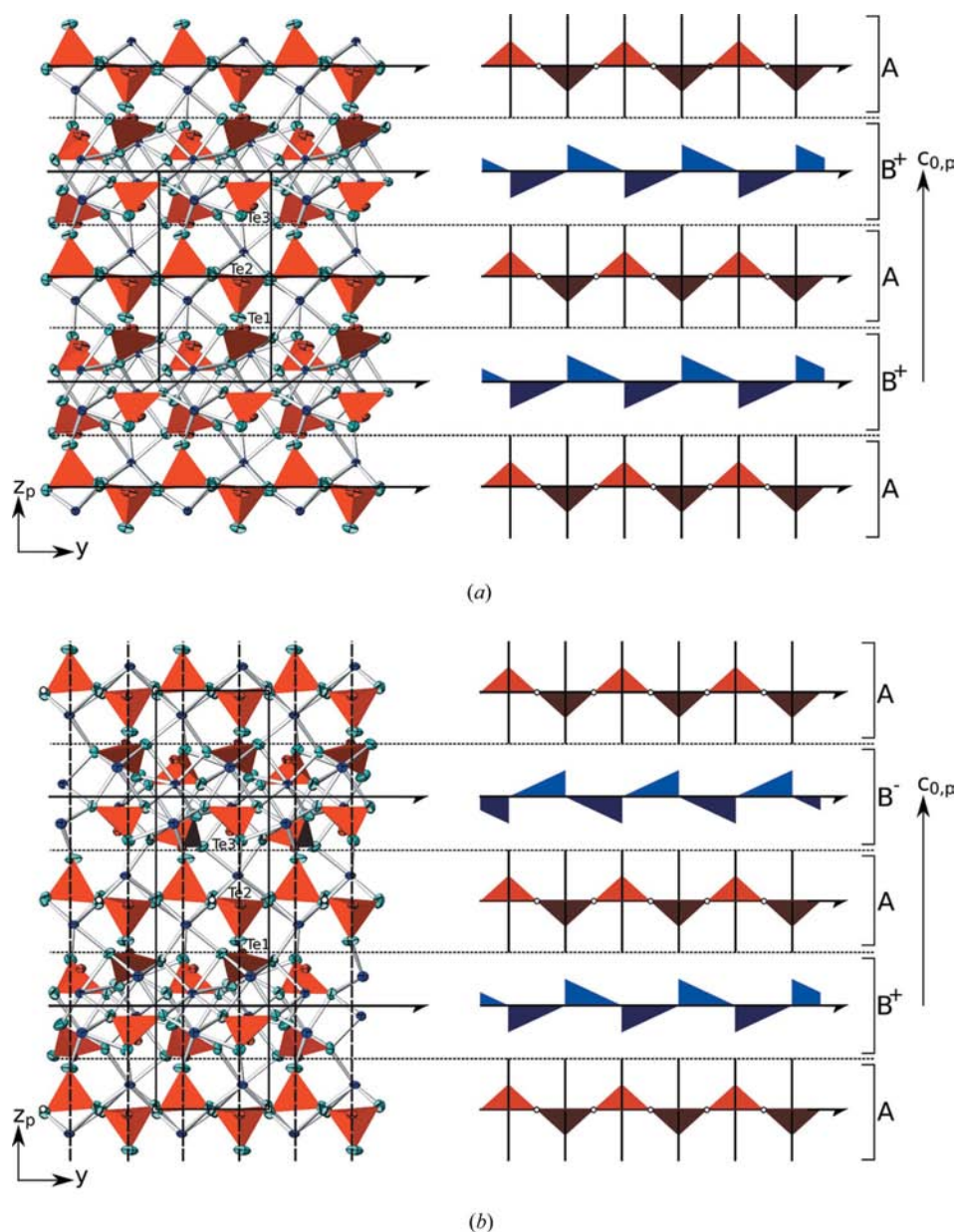
All polytypes exhibit oval channels (smallest and largest diameter ~ 2 and 8 Å) running along [010], delimited by six [Te^{IV}O₃]²⁻ units (Fig. 5). The long and short diameters of the channels are parallel to [001] and [100]. [MO]_x ($M = \text{Ca, Sr}$) polyhedra ($x = 7-8$) are located around the channels and connect the [Te^{IV}O₃]²⁻ units *via* corners and edges. The lone-pair electrons of the Te^{IV} atoms are directed towards the channels (Fig. 5).

3.3.3. Positional disorder in Ca_xSr_{1-x}TeO₃. There is considerably more substitution by Sr in one of the three different Ca positions (Ca1) (Table 9) than in the others. As expected, the Ca–O distances increase with the amount of substitution (Table 7). Even in unsubstituted γ -CaTeO₃, the Ca–O distances are slightly larger for Ca1 than for Ca2 and Ca3, indicating more space at the Ca1 position required for larger atoms when substituted.

3.4. β - and β' -CaTeO₃

3.4.1. Data collection. Multiple heating/cooling cycles of a β -CaTeO₃ crystal mounted on a single-crystal diffractometer have shown that β -CaTeO₃ slowly transforms to a low-

² Supplementary data for this paper are available from the IUCr electronic archives (Reference: SN5078). Services for accessing these data are described at the back of the journal.


Figure 4

(a) MDO₁ and (b) MDO₂ polytypes of γ -CaTeO₃ and Ca_xSr_{1-x}TeO₃, viewed down [100]. To the right the schematized OD structure is represented by red triangles with a mirror plane normal to [010] and by blue triangles without a mirror plane. Bright and dark colours symbolize the front and the back side of the triangles. Letters to the right describe the layer type. Colour codes, displacement ellipsoids and symbols as in Fig. 2. A subscript 'p' designates a coordinate axis which does not lie in the drawing plane (Hahn, 1983).

temperature phase β' -CaTeO₃ at temperatures below ~ 270 K with distinctly different lattice parameters. To obtain single phase β' -CaTeO₃, the crystal had to be cooled for a few hours at 200 K. When the measurements were started shortly after cooling, the reflections showed considerable splitting, which can be attributed to simultaneous existence of β - as well as β' -CaTeO₃.

The inverse transition β' -CaTeO₃ \rightarrow β -CaTeO₃ occurred instantly when heating the crystal at ~ 300 K. Due to this large hysteresis it was possible to avoid a spontaneous phase transition and collect data for both β - and β' -CaTeO₃

phases using the same crystal for measurement at 275 K, by cooling from 300 K and by heating from 200 K.

3.4.2. Structure refinement. The lattice parameters of β - and β' -CaTeO₃ clearly indicate a triclinic crystal system. While β' -CaTeO₃ crystallizes without doubt in $P\bar{1}$, the situation for β -CaTeO₃ is not so clear. Refinements of β -CaTeO₃ always resulted in satisfactory and comparable *R* values for structure models in *P1* as well as in $P\bar{1}$. The structure models obtained by refinements in *P1* and in $P\bar{1}$ are practically equivalent with the exception of one O atom, which is disordered around a symmetry centre. For measurements at 275 and 295 K, refinements in *P1* gave distinctly better reliability factors than in $P\bar{1}$. For datasets collected at 325 and 350 K, the situation was reversed: refinements in $P\bar{1}$ gave better *R* values than refinements in *P1*. The determined structures were practically identical to those obtained at lower temperatures though. Fig. 6 gives a survey of the lattice parameters and space groups of β - and β' -CaTeO₃ at different temperatures.

For the dataset of the β -CaTeO₃ phase collected at 275 K, the O atoms were refined with isotropic temperature factors since the ADPs were highly anisotropic, one O atom even giving physically meaningless values. We attribute this behavior to the kinetically inhibited phase transition β -CaTeO₃ \rightarrow β' -CaTeO₃ in this temperature

range.

Instead of the reduced unit-cell setting³ an unusual setting [$a \approx 25.6$, $b \approx 10.4$, $c \approx 11.2$ Å, $\alpha \approx 107.2$, $\beta \approx 110.3$, $\gamma \approx 33.0^\circ$] was chosen in order to highlight the threefold superstructure of β - and β' -CaTeO₃ and the close similarity to the OD structures of γ -CaTeO₃ and Ca_xSr_{1-x}TeO₃.

³ The reduced cell of β -CaTeO₃ at 295 K is $a = 10.2355$ (4), $b = 11.3248$ (4), $c = 13.9877$ (5) Å, $\alpha = 78.469$ (1), $\beta = 85.928$ (1), $\gamma = 72.793$ (1) $^\circ$. The transformation matrix that relates the reduced cell to the used setting is $(-2 \ -1 \ 0 \ 0 \ 0 \ 1 \ -1 \ 0 \ 0)$.

Table 7

Selected atomic distances (Å) and angles (°) in γ -CaTeO₃ (MDO₁ and MDO₂) and Ca_xSr_{1-x}TeO₃.

For MDO₂ only atoms in layer *B* are considered, since atoms in layer *A* were not refined separately for both polytypes.

	γ -CaTeO ₃ , MDO ₁	γ -CaTeO ₃ , MDO ₂	Ca _{0.77} Sr _{0.23} TeO ₃	Ca _{0.55} Sr _{0.45} TeO ₃
Te1—O3	1.859 (6)	1.87 (4)	1.866 (3)	1.866 (3)
Te1—O1	1.868 (5)	1.88 (4)	1.862 (3)	1.862 (3)
Te1—O2	1.872 (5)	1.86 (4)	1.870 (3)	1.867 (3)
Te2—O6	1.834 (4)	—	1.833 (4)	1.831 (4)
Te2—O4	1.840 (4)	—	1.841 (3)	1.836 (3)
Te2—O5	1.852 (4)	—	1.858 (4)	1.857 (4)
Te3—O7	1.838 (5)	1.90 (3)	1.859 (3)	1.858 (3)
Te3—O9	1.841 (12)	1.94 (5)	1.853 (3)	1.858 (3)
Te3—O8	1.875 (5)	1.78 (4)	1.864 (3)	1.865 (3)
Ca1—O4	2.340 (4)	—	2.389 (3)	2.433 (4)
Ca1—O8	2.392 (5)	2.41 (4)	2.455 (3)	2.495 (3)
Ca1—O8	2.419 (5)	2.44 (4)	2.498 (3)	2.547 (3)
Ca1—O9	2.429 (6)	2.48 (5)	2.528 (3)	2.585 (4)
Ca1—O1	2.538 (5)	2.54 (4)	2.600 (3)	2.643 (3)
Ca1—O7	2.669 (6)	2.56 (4)	2.708 (3)	2.733 (3)
Ca1—O7	2.702 (6)	2.72 (3)	2.712 (3)	2.741 (3)
Ca1—O2	2.785 (6)	2.72 (4)	2.750 (4)	2.767 (4)
Ca2—O6	2.322 (4)	—	2.337 (4)	2.358 (4)
Ca2—O9	2.339 (12)	—	2.350 (3)	2.387 (3)
Ca2—O5	2.339 (4)	—	2.344 (4)	2.368 (4)
Ca2—O1	2.393 (5)	—	2.387 (3)	2.405 (3)
Ca2—O6	—	—	2.337 (4)	2.575 (4)
Ca2—O5	—	—	2.344 (4)	2.636 (4)
Ca2—O2	2.517 (6)	—	2.638 (4)	2.676 (4)
Ca3—O7	2.220 (5)	2.21 (3)	2.251 (3)	2.285 (3)
Ca3—O3	2.292 (6)	2.35 (4)	2.305 (3)	2.323 (3)
Ca3—O2	2.297 (5)	2.24 (4)	2.322 (3)	2.347 (3)
Ca3—O8	2.467 (5)	2.53 (4)	2.480 (3)	2.488 (3)
Ca3—O3	2.521 (6)	2.45 (4)	2.532 (3)	2.561 (3)
Ca3—O1	2.550 (6)	2.58 (4)	2.572 (3)	2.608 (4)
Ca3—O9	3.019 (14)	3.12 (6)	3.068 (3)	3.069 (3)
O1—Te1—O2	93.4 (2)	93.0 (17)	93.73 (16)	94.11 (16)
O1—Te1—O3	92.2 (2)	89.0 (18)	91.95 (14)	91.87 (15)
O2—Te1—O3	103.5 (3)	99.4 (18)	102.45 (15)	101.89 (16)
O4—Te2—O5	103.27 (18)	—	93.47 (16)	103.40 (18)
O4—Te2—O6	103.43 (18)	—	102.99 (17)	103.04 (19)
O5—Te2—O6	93.10 (18)	—	103.36 (17)	93.18 (17)
O7—Te3—O8	94.1 (2)	91.3 (16)	93.94 (13)	94.60 (14)
O7—Te3—O9	90.2 (3)	94.2 (17)	91.44 (14)	91.94 (14)
O8—Te3—O9	99.4 (4)	104 (2)	99.53 (15)	99.10 (15)

The basis vectors **a**, **b** and **c** of β - and β' -CaTeO₃ can be approximated by the basis vectors **a'**, **b'** and **c'** of the MDO₁ polytype of γ -CaTeO₃ by

$$(\mathbf{a}, \mathbf{b}, \mathbf{c}) \simeq (\mathbf{a}', \mathbf{b}', \mathbf{c}') \begin{pmatrix} 3 & 1 & 0 \\ 0 & 1 & 0 \\ 0 & 0 & 1 \end{pmatrix}.$$

Therefore, the volume of the unit cell of β - and β' -CaTeO₃ is approximately three times that of MDO₁ of γ -CaTeO₃. The relationship between the unit cells of β - and β' -CaTeO₃ and both γ -CaTeO₃ polytypes is represented in Fig. 7.

The labelling of the atoms has been assigned consistently with the γ -CaTeO₃ polymorphs: The numbers of the Te and Ca atoms in β - and β' -CaTeO₃ consist of two digits, the first digit being the same as of the corresponding atom in γ -CaTeO₃. In the following discussion, we will write Te1*x* for all or a subset

Table 8

Deviations (Å) of the real structure atoms in layer *A* in γ -CaTeO₃ and Ca_xSr_{1-x}TeO₃ from the corresponding atoms in the idealized structure.

Atom	γ -CaTeO ₃	Ca _{0.77} Sr _{0.23} TeO ₃	Ca _{0.55} Sr _{0.45} TeO ₃
Te1	0.102	0.012	0.019
Te2	0.032	0.067	0.074
Ca2	0.108	0.054	0.055
O4	0.098	0.241	0.267
O5, O6	0.123	0.169	0.183

of the atoms corresponding to atom Te1 in γ -CaTeO₃ and *mutatis mutandis* for other heavy atoms.

The O atoms have been labelled according to the connectivity to the Te atoms: The first digit was chosen so that the first digit of all atoms in the [TeO₃]²⁻ units relate to those of the

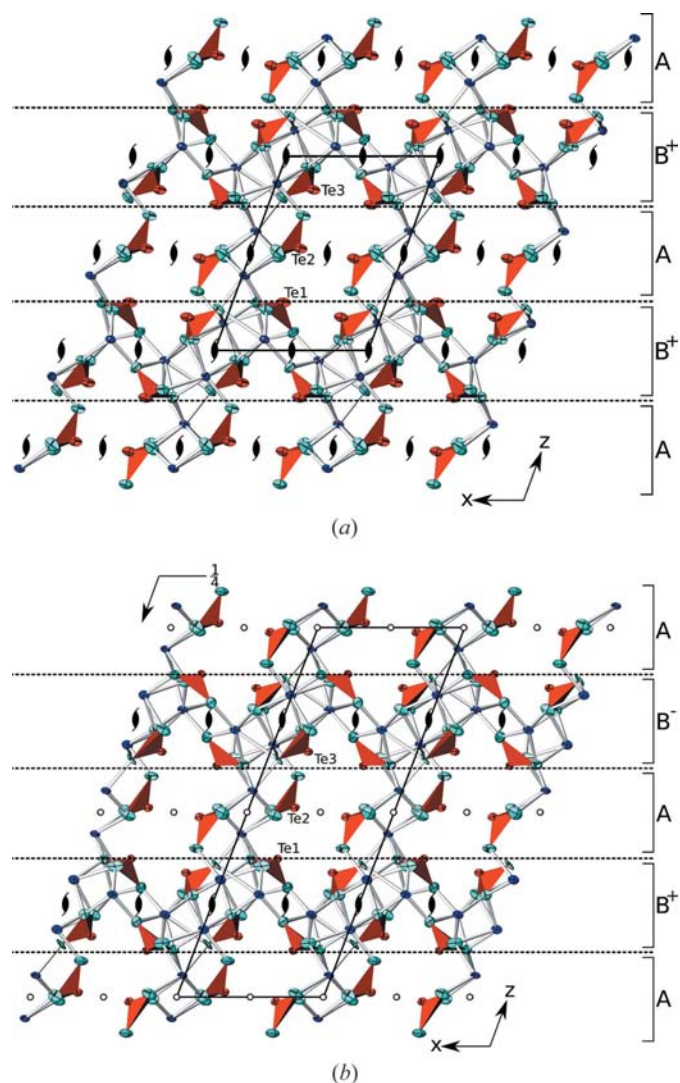
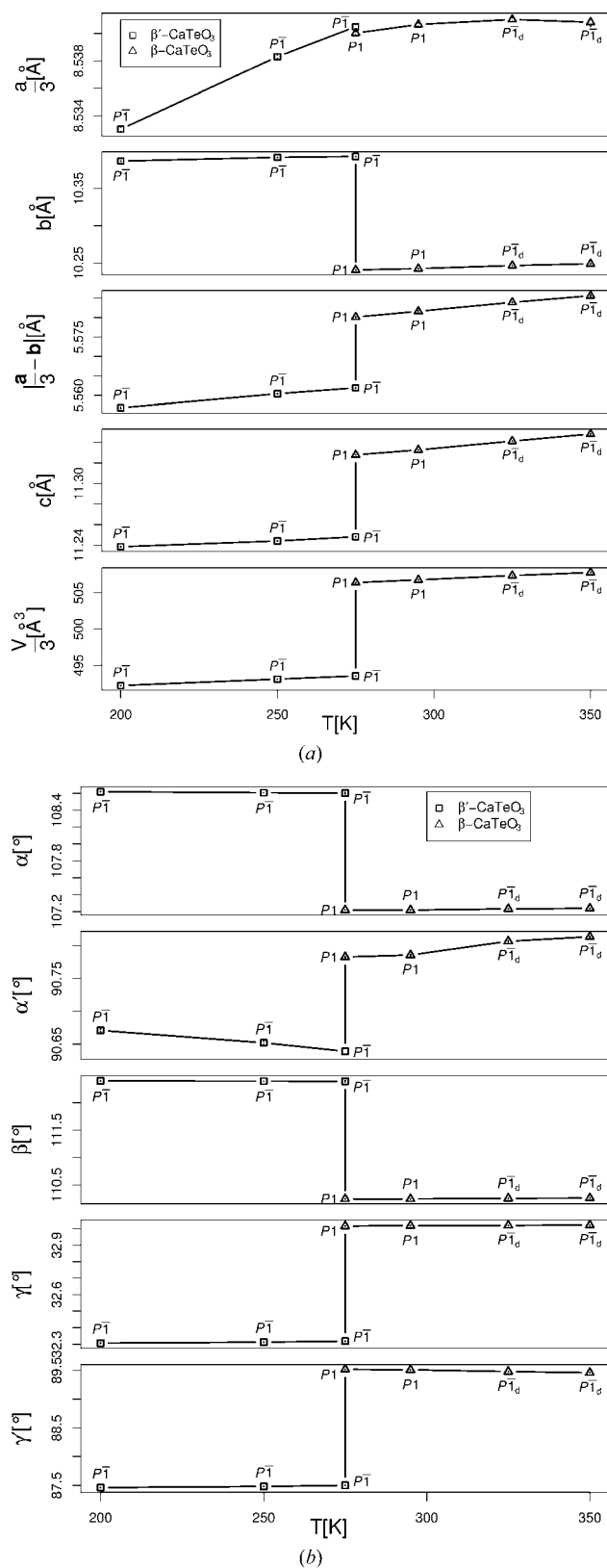


Figure 5 Representations of (a) the MDO₁ and (b) the MDO₂ polytype of γ -CaTeO₃ and Ca_xSr_{1-x}TeO₃, viewed down [010]. MDO₁ is represented by the crystal structure of Ca_{0.77}Sr_{0.23}TeO₃, MDO₂ by the main polytype of γ -CaTeO₃. Letters to the right describe the layer type. A superscript '+' or '-' besides layers of type *B* indicates its orientation with respect to [010]. Colour codes, displacement ellipsoids and symbols as in Fig. 2.


Figure 6

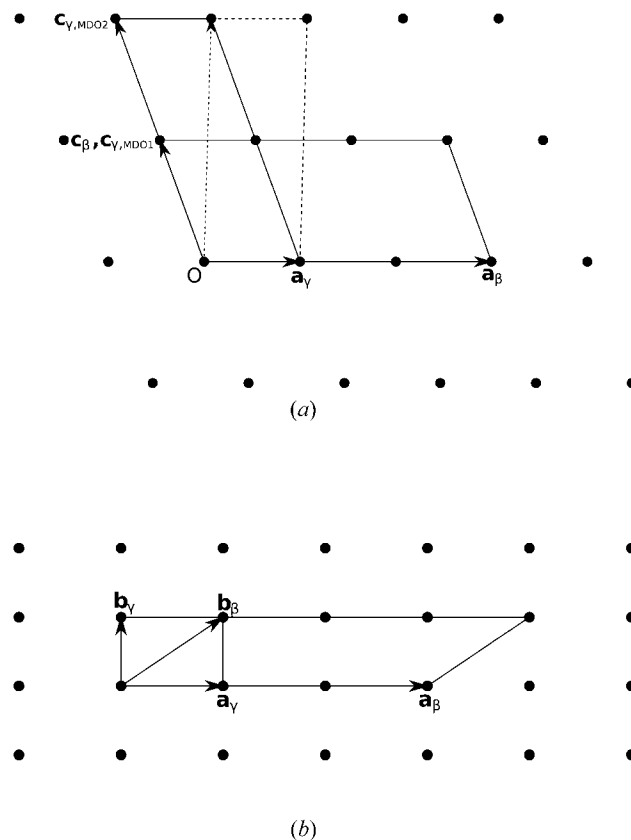
Variation of (a) lattice parameters a , b , c , $b' \equiv \frac{1}{3}|\mathbf{a} - \mathbf{b}|$ and cell volume, and (b) the angles α , $\alpha' = \mathbf{b}' \cdot \mathbf{c}$, β , γ , $\gamma' = \mathbf{a} \cdot \mathbf{b}'$ of β - and β' - CaTeO_3 with temperature. Measurements of β - and β' - CaTeO_3 are indicated by triangles and squares. The text next to the symbol indicates the space group, a subscript 'd' meaning a disordered structure. Error bars have been omitted since they are smaller than the symbol sizes.

corresponding unit in γ - CaTeO_3 . Thus, since Te1 connects to O1–O3 in γ - CaTeO_3 , Te1 x connects to O1 x , O2 x and O3 x in β - and β' - CaTeO_3 etc.

3.4.3. Structure. β - and β' - CaTeO_3 are threefold superstructures along $[100]$ based on the MDO_1 polytype description of γ - CaTeO_3 . Although the symmetry conditions given for layers A and B in the description of γ - CaTeO_3 do not hold anymore, it is still useful to distinguish between those layers for comparison with γ - CaTeO_3 (Fig. 8).

Due to the superstructure, β - and β' - CaTeO_3 can be described as being composed of three different non-translational equivalent rods with pseudo-monoclinic metrics (Table 10), running along $[001]$ (Fig. 9). Each rod consists of a stacking of distorted γ - CaTeO_3 MDO_1 unit cells.

In β' - CaTeO_3 two types of rods can be differentiated, which we denote by C' and D . Rods of type C' are centrosymmetric (rod group symmetry $\mu\bar{1}$), whereas rods of type D are non-centrosymmetric (rod group symmetry $\mu 1$) and can appear in two enantiomorphic orientations (D^+ and D^-). The rods extend along $[100]$ (and $[\bar{1}\bar{3}0]_\beta \hat{=} [010]_\gamma$) according to: $\dots D^+ CD^- D^+ CD^- \dots$ (Fig. 9, right), resulting in a structure with overall $P\bar{1}$ symmetry.


Figure 7

Relationship of the unit cells of β - CaTeO_3 and the γ - CaTeO_3 polytypes MDO_1 and MDO_2 . The dots represent the crystal lattice of the MDO_1 polytype in γ - CaTeO_3 . (a) Projection on (010) ; (b) projection on (001) . \mathbf{a}_β is tripled when compared with \mathbf{a}_γ owing to the threefold superstructure of β - CaTeO_3 along $[100]$. $\mathbf{c}_{\gamma, \text{MDO}_1}$ is doubled when compared with $\mathbf{c}_{\gamma, \text{MDO}_2}$. The dotted lines in the left part represent the reduced setting of the unit cell of γ - CaTeO_3 MDO_2 with pseudo-orthorhombic metric.

When compared with MDO_1 of γ - $CaTeO_3$, one of two $[Te_2xO_3]^{2-}$ units of rods D is rotated by $ca\ 45^\circ$, removing the mirror plane of layer A. One $[Te_1xO_3]^{2-}$ unit, which lies

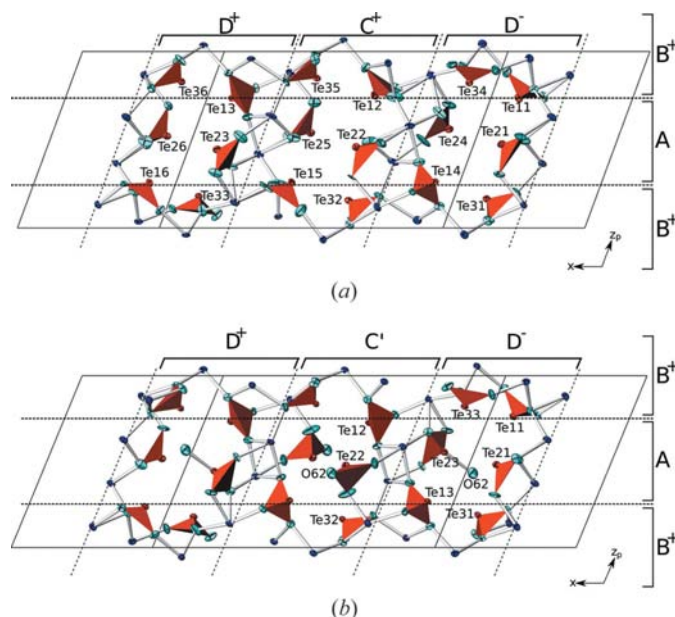


Figure 8
The unit-cell contents of the crystal structures of (a) β - $CaTeO_3$ ($P1$) and (b) β' - $CaTeO_3$ ($P1$) measured at 295 and at 200 K, projected along $[1\bar{3}0]$ exemplifying the threefold superstructure along $[100]$. Colour codes, displacement ellipsoids and symbols as in Fig. 2. The layer type according to the OD description of γ - $CaTeO_3$ is denoted by letters to the right. Letters at the top denote the rod type.

Table 9

Ca substitution in the phases $Ca_xSr_{1-x}TeO_3$.

Ca:Sr ratio used in synthesis	1:1	2:1
Single crystal data		
Sum formula	$Ca_{0.55}Sr_{0.45}TeO_3$	$Ca_{0.77}Sr_{0.23}TeO_3$
a (Å)	8.5689 (17)	8.4941 (6)
b (Å)	5.7805 (11)	5.7368 (4)
c (Å)	11.553 (2)	11.4562 (8)
β ($^\circ$)	109.975 (3)	110.0810 (10)
Ca1:Sr1	31.1:68.9 (4)	60.0:40.0 (5)
Ca2:Sr2	63.7:36.3 (4)	83.8:16.2 (4)
Ca3:Sr3	71.3:28.6 (4)	87.5:12.5 (4)

entirely in layer B in γ - $CaTeO_3$, is rotated so that one O atom moves from layer B to layer A (Fig. 10).

The centrosymmetric subcell C' in β' - $CaTeO_3$ shows more deviation from MDO_1 . Both $[Te_1xO_3]^{2-}$ units are moved partly into layer A. The $[Te_2xO_3]^{2-}$ units of layer A are tilted so that one O atom (O62) is no longer connected to a Ca atom, but is instead located in the channel. O62 is located $\simeq 2.47$ Å from Te23 in the next subcell in the $[1\bar{3}0]$ direction on the opposite side of the channel, giving the only $[3+1]$ coordination of any Te atom and the only corner-sharing between two $[TeO_4]$ units of all structures presented in this work. The Te–O distances in this $[TeO_{3+1}]$ polyhedron are typical for this kind of coordination, which is, for example, also found in the structures of $Zn_2Te_3O_8$, Te_2MoO_7 , $CuTeO_3$ and $CuTe_2O_5$ (Arnaudov *et al.*, 1982).

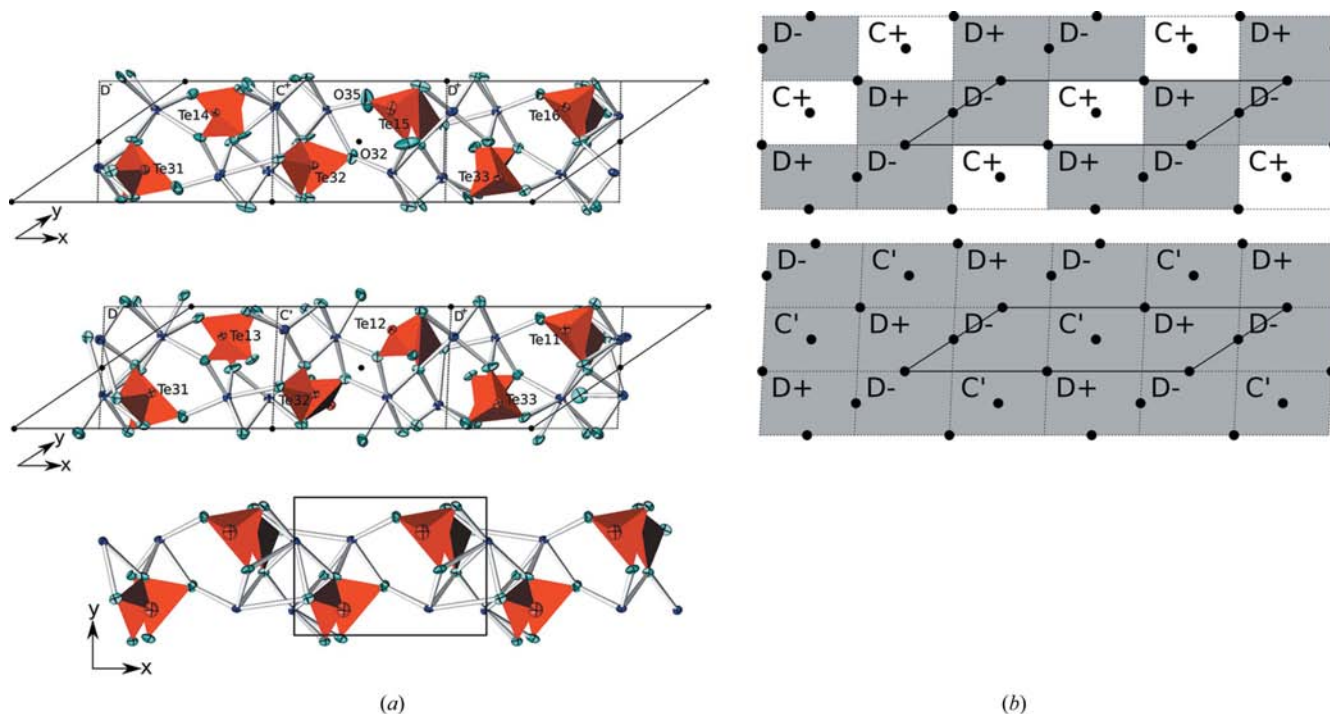


Figure 9
(a) Layer B of β -, β' - $CaTeO_3$ and $Ca_xSr_{1-x}TeO_3$ viewed down $[001]$. Colour codes and displacement ellipsoids as in Fig. 2. Dots symbolize centres of (pseudo-)inversion symmetry. Top row: β - $CaTeO_3$. The pair of O atoms breaking pseudo-inversion symmetry (O32/O35) is labelled. Middle row: β' - $CaTeO_3$. Bottom row: $Ca_xSr_{1-x}TeO_3$. (b) Symbolic arrangement of different type of rods. Rods with a grey background belong to the centrosymmetric parts of the structures.

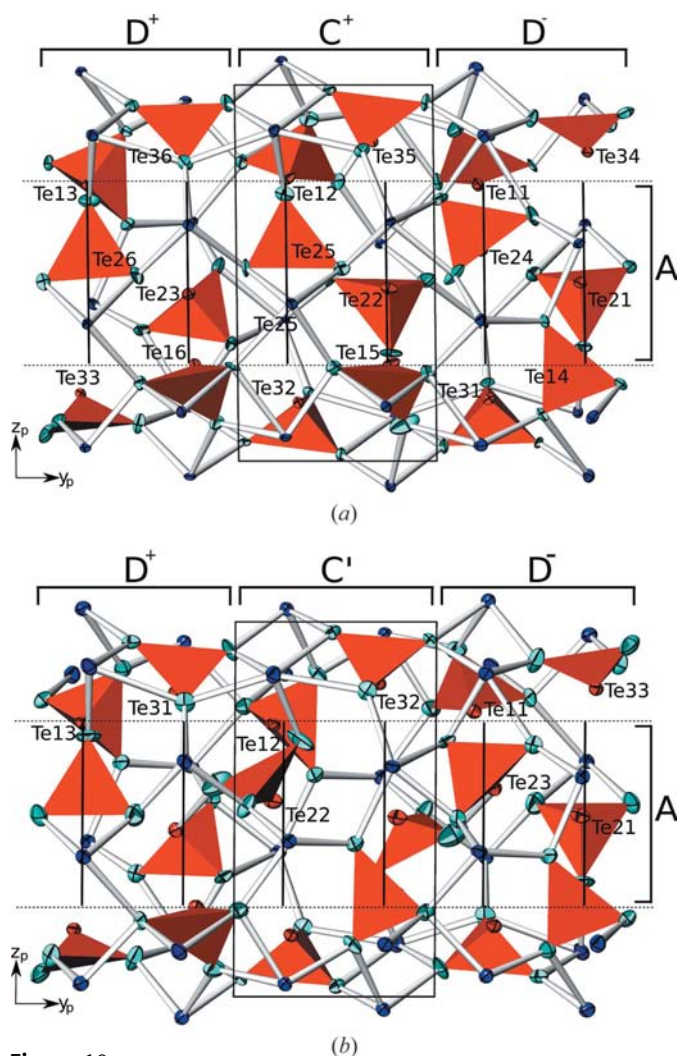
Table 10

 Comparison of the pseudo-monoclinic metrics of the subcells in β - and β' -CaTeO₃ measured at different temperatures with the cell parameters of MDO₁ of γ -CaTeO₃.

Compound	β' -CaTeO ₃	β' -CaTeO ₃	β' -CaTeO ₃	β -CaTeO ₃	β -CaTeO ₃	β -CaTeO ₃	β -CaTeO ₃	γ -CaTeO ₃ (MDO ₁)
<i>T</i> (K)	200	250	275	275	295	325	350	295
<i>a</i> (Å)	8.5330 (2)	8.5383 (1)	8.5405 (1)	8.5400 (1)	8.5407 (3)	8.5410 (1)	8.5408 (3)	8.4010 (17)
<i>b</i> (Å)	5.5568 (2)	5.5604 (1)	5.5619 (1)	5.5801 (1)	5.5816 (2)	5.5839 (1)	5.5856 (2)	5.6913 (11)
<i>c</i> (Å)	11.2384 (3)	11.2440 (2)	11.2481 (1)	11.3279 (2)	11.3327 (4)	11.3413 (2)	11.3482 (4)	11.340 (3)
α (°)	90.671 (2)	90.652 (2)	90.639 (5)	90.783 (1)	90.786 (1)	90.807 (1)	90.814 (1)	90
β (°)	112.398 (1)	112.394 (2)	112.393 (7)	110.245 (1)	110.245 (1)	110.255 (1)	110.260 (1)	110.82 (3)
γ (°)	87.461 (1)	87.480 (1)	87.499 (1)	89.517 (1)	89.511 (1)	89.480 (1)	89.460 (1)	90
<i>V</i> (Å ³)	492.20 (2)	493.08 (2)	493.53 (2)	506.43 (2)	506.81 (3)	507.40 (2)	507.82 (3)	506.8 (2)

In β -CaTeO₃ the centrosymmetric rods *C'* of β' -CaTeO₃ are replaced by pseudo-centrosymmetric rods which we denote by *C* (*A*) and which can appear in two enantiomorphic orientations (*C*⁺ and *C*⁻). In *P*1 refinements, only one orientation exists, whereas in *P* $\bar{1}$ both orientations appear in a disordered manner.

Rods of type *C* in β -CaTeO₃ are closely related to the unit cell of the MDO₁ polytype in γ -CaTeO₃. The atoms in layer *A* show only slight deviation from those in γ -CaTeO₃. In layer *B*, one of the [Te₃xO₃]²⁻ units is rotated, so that the two [Te₃xO₃]²⁻ units are related by (pseudo-)inversion symmetry, but break the 2₁ symmetry of γ -CaTeO₃. The [Te1xO₃]²⁻ units, on the other hand, retain the position from MDO₁, fulfilling 2₁ symmetry, but breaking inversion symmetry. In Fig. 9 the units that used to be part of layer *B* are shown projected along [001], the O atoms breaking inversion symmetry being highlighted. Rod *C* can therefore be seen as an intermediate step in a *P* $\bar{1}$ → *P*2₁ transition from β' -CaTeO₃ to γ -CaTeO₃, which is not yet confirmed.


Figure 10

Slabs of (a) β - and (b) β' -CaTeO₃ viewed down [100]. Colour codes and displacement ellipsoids as in Fig. 2. The middle part corresponds to layer *A* of γ -CaTeO₃. Black, nearly vertical lines represent the mirror planes of the idealized structure of layer *A*.

3.5. Lattice parameters of β - and β' -CaTeO₃ versus temperature

Due to the superstructure of β - and β' -CaTeO₃ not only the lattice parameters but also those of the subcells corresponding to the lattice parameters of γ -CaTeO₃: $b' = |\mathbf{b}'| = |\frac{1}{3}\mathbf{a} - \mathbf{b}|$, $\alpha' = \mathbf{b}' \cdot \mathbf{c}$ and $\gamma' = \mathbf{a}, \mathbf{b}'$ and their relation to those of γ -CaTeO₃ were analysed.

The cell volume of β - and β' -CaTeO₃ increases linearly with temperature (Fig. 6, left) as do the lattice parameters *b*, *b'* and *c*. *a*, on the other hand, increases linearly only in β' -CaTeO₃, whereas in β -CaTeO₃ the increase is less marked and *a* even reaches a maximum at 325 K (Fig. 6, left). The angles of the subcell α' , β and γ' all show the opposite behaviour in β - and β' -CaTeO₃: α' and β decrease with temperature in β' and increase in β -CaTeO₃, γ' increases in β' - and decreases in β -CaTeO₃ (Fig. 6, right).

The phase transition β' -CaTeO₃ → β -CaTeO₃ is marked by a distinct jump in lattice parameters as can be seen by comparison of the lattice parameters of both phases measured at 275 K: The cell volume increases from 1480.59 (5) to 1519.28 (5) Å³, *c* increases from 5.5619 (1) to 5.5801 (1) Å, whereas *b* decreases from 10.3933 (2) to 10.2408 (2) Å. This can be associated with an increase of γ' by over 2° from 87.499 (1) to 89.517 (1)°, resulting in a pseudo-monoclinic metric of the subcell, and thus a shortening of the diagonal of the basis of the subcell. *a* stays practically equal for β - and β' -CaTeO₃ at 275 K. *b'* jumps significantly from 5.5619 (1) to 5.5801 (1) Å showing stretching of the structure in the direction of the channels. α' slightly increases from 90.639 (5) to 90.783 (5)°. β decreases from 112.392 (7) to 110.245 (1)°, the

latter being closer to the corresponding angle in γ -CaTeO₃ [110.82 (3)°]. Finally, γ' jumps by over 2° from 87.499 (1) to 89.517 (1)°.

4. Results and discussion

The structures of four CaTeO₃ polymorphs and of the solid solutions Ca_xSr_{1-x}TeO₃ have been solved. The thermodynamically stable CaTeO₃ phase at room temperature, α -CaTeO₃, is structurally unrelated to the high-temperature phases β -, β' - and γ -CaTeO₃, which are all based on the same structure principles. The basic structure of the high-temperature phases is the monoclinic non-centrosymmetric MDO₁ polytype of γ -CaTeO₃. The second (major) polytype of γ -CaTeO₃, MDO₂, has a doubled periodicity in the direction of the layer stacking. Ca_xSr_{1-x}TeO₃ is isostructural to MDO₁. The triclinic polymorphs β - and β' -CaTeO₃ can be interpreted as a threefold superstructure of MDO₁ along [100] and [010] of MDO₁. While β' -CaTeO₃ is centrosymmetric, in β -CaTeO₃ one of three subcells partly takes the configuration of non-centrosymmetric MDO₁ and β -CaTeO₃ can therefore be seen as an intermediate step in a possible β' -CaTeO₃ → γ -CaTeO₃ transition, which is not yet observed.

In supplementary DSC experiments, the reconstructive phase transformation α → β was determined to occur at 1170 (5) K, the melting point of CaTeO₃ at 1340 (5) K. The β to γ ratio obtained in different batches from melts varied notably, but so far we have been unable to fully understand all the factors that come into play, such as the heating program, sample size and crucible material for synthesis, for the preparation of a single-phase material. A more detailed investigation of the stability ranges of the different CaTeO₃ polymorphs is in preparation, with special attention paid to the formation conditions of β - and γ -CaTeO₃ and the MDO₁ and MDO₂ polytypes of γ -CaTeO₃.

The endothermic phase transition $\beta' \rightarrow \beta$ is sharp and occurs at ~293 K, whereas the reverse phase transition $\beta \rightarrow \beta'$ is kinetically inhibited, ranging from 273 to 233 K when cooling at 5 K s⁻¹. Since no other CaTeO₃ polymorph we investigated showed any phase transition in this temperature range, the ferroelectric phase transition in this temperature range reported by Rai *et al.* (2002) seems to originate from the β polymorph.

None of the three CaTeO₃ polymorphs indexed by Mishra *et al.* (1998) correspond to any of the α , β , β' or γ -CaTeO₃ phases reported here. The major reflections in the powder diffraction pattern of ' α -CaTeO₃' obtained by Mishra *et al.* (1998) can be assigned to a mixture of the Te-rich phase Ca₄Te₅O₁₄ and α -CaTeO₃, whereas the origin of the reflections of ' β -' and ' γ -CaTeO₃' remains unclear. Temperature-dependent XRPD experiments of single-phase CaTeO₃ samples are planned for the near future.

In comparison with the structures of the homologous SrTeO₃ polymorphs (Zavodnik *et al.*, 2007a,b,c, 2008), the CaTeO₃ structures discussed here bear similarities in the basic building units. All four SrTeO₃ polymorphs crystallize in

monoclinic space groups and are likewise made up from MO_x (M = Sr, x = 7–8) and isolated trigonal-prismatic [TeO₃]²⁻ units, linked together to form channels that for all structures run down [010]. As in the CaTeO₃ structures, the channels provide space that is required for the electron lone pairs of the [TeO₃]²⁻ units. However, the connection of the MO_x and [TeO₃]²⁻ units differs significantly between the Ca and Sr phases, leading to entirely different structures.

The authors wish to thank Dr Ekkehard Füglein (Netzsch, Germany) for carrying out the thermal analyses and the FWF (Fonds zur Förderung der wissenschaftlichen Forschung) for financial support (project No. P19099-N17).

References

- Arnaudov, M., Dimitrov, V., Dimitriev, Y. & Markova, L. (1982). *Mater. Res. Bull.* **17**, 1121–1129.
- Barrier, N., Rueff, J. M., Lepetit, M. B., Contreras-Garcia, J., Malo, S. & Raveau, B. (2008). *Solid State Sci.*, doi: 10.1016/j.solidstatesciences.2008.09.014.
- Bruker (2004). *APEX, SMART, SADABS*. Bruker Analytical X-ray Instruments Inc., Madison, Wisconsin, USA.
- Burckhardt, H.-G., Platte, C. & Trömel, M. (1982). *Acta Cryst.* **B38**, 2450–2452.
- Dityatiev, O. A., Berdonosov, P. S., Dolgikh, V. A., Aldous, D. W. & Lightfoot, P. (2006). *Solid State Sci.* **8**, 830–835.
- Dolgikh, V. A. (1991). *Russ. J. Inorg. Chem.* **36**, 1117–1129.
- Dornberger-Schiff, K. & Grell, H. (1982). *Acta Cryst.* **A38**, 491–498.
- Durović, S. (1997). *EMU Notes Miner.* **1**, 3–28.
- Effenberger, H., Zemann, J. & Mayer, H. (1978). *Am. Mineral.* **63**, 847–852.
- Elerman, E. (1993). *Doga. Turk. J. Phys.* **17**, 465–473.
- Ferraris, G., Makovicky, E. & Marlino, S. (2004). *Crystallography of Modular Materials*. Oxford University Press.
- Flack, H. D. (1983). *Acta Cryst.* **A39**, 876–881.
- Grell, H. & Dornberger-Schiff, K. (1982). *Acta Cryst.* **A38**, 49–54.
- Hahn, T. (1983). Editor. *International Tables for Crystallography*, Vol. A. Dordrecht: D. Reidel Publishing Company.
- Hottentot, D. & Loopstra, B. O. (1979). *Acta Cryst.* **B35**, 728–729.
- Hottentot, D. & Loopstra, B. O. (1981). *Acta Cryst.* **B37**, 220–222.
- Ivankova, E. A., Samplavskaya, K. K., Malyutin, M. K. & Mendeleev, D. I. (1966). *Izv. Akad. Nauk. SSSR Neorg. Mater.* **2**, 896–898.
- Knyaceva, R. N. & Gushchina, A. S. (1968). *Zh. Neorg. Chim.* **13**, 1506–1509.
- Kopsky, V. & Litvin, D. B. (2002). Editors. *International Tables for Crystallography*, Vol. E. Dordrecht: Kluwer Academic Publishers.
- Malyutin, S. A., Samplavskaya, K. K. & Karapet'yants, M. K. (1969). *J. Alloys Compds*, **280**, 56–64.
- Mishra, R., Namboodiri, P. N., Tripathi, S. N. & Dharwadkar, S. R. (1998). *J. Alloys Compds*, **280**, 56–64.
- Otwinowski, Z., Borek, D., Majewski, W. & Minor, W. (2003). *Acta Cryst.* **A59**, 228–234.
- Rai, R., Sharma, S. & Choudhary, R. N. P. (2002). *J. Mater. Sci. Lett.* **21**, 297–299.
- Redman, M. J., Chen, J. H., Binnie, W. P. & Mallio, W. J. (1970). *J. Am. Ceram. Soc.* **53**, 645–648.
- Rodriguez-Carvajal, J. (1993). *FULLPROF*, Version 3.3. Laboratoire Léon Brillouin, Saclay, France.
- Shannon, R. D. (1976). *Acta Cryst.* **A32**, 751–767.
- Sheldrick, G. M. (2008). *Acta Cryst.* **A64**, 112–122.
- Tripathi, S. N., Mishra, R., Mathews, M. D. & Namboodiri, P. N. (2001). *Powder Diffr.* **16**, 205–211.

- Trömel, M. & Ziethen-Reichenach, H. (1970). *Z. Anorg. Allg. Chem.* **378**, 232–237.
- Weil, M. (2004). *Solid State Sci.* **6**, 29–37.
- Weil, M. & Stöger, B. (2008). *Acta Cryst.* **C64**, i79–i81.
- Wroblewska, J., Erb, A., Dobrowolski, J. & Freundlich, W. (1979). *Rev. Chim. Mineral.* **16**, 112–123.
- Yamada, T. (1975). *Rev. Electr. Somm. Lab.* **23**, 564–568.
- Yamada, T. & Iwasaki, H. (1972). *Appl. Phys. Lett.* **21**, 89–90.
- Zavodnik, V. E., Ivanov, S. A. & Stash, A. I. (2007a). *Acta Cryst.* **E63**, i75–i76.
- Zavodnik, V. E., Ivanov, S. A. & Stash, A. I. (2007b). *Acta Cryst.* **E63**, i151.
- Zavodnik, V. E., Ivanov, S. A. & Stash, A. I. (2007c). *Acta Cryst.* **E63**, i111–i112.
- Zavodnik, V. E., Ivanov, S. A. & Stash, A. I. (2008). *Acta Cryst.* **E64**, i52.
- Zemann, J. (1971). *Monatsh. Chem.* **102**, 1209–1216.